One-Shot Deep-UV Pulsed-Laser-Induced Photomodification of Hollow Metal Nanoparticles for High-Density Data Storage on Flexible Substrates

Dehui Wan,[†] Hsuen-Li Chen,[†,*] Shao-Chin Tseng,[†] Lon A. Wang,[‡] and Yung-Pin Chen[‡]

[†]Department of Materials Science and Engineering, and [‡]Department of Electrical Engineering and Graduate Institute of Photonics and Optoelectronics, National Taiwan University, Taipei, Taiwan

ABSTRACT In this paper, we report a new optical data storage method: photomodification of hollow gold nanoparticle (HGN) monolayers induced by one-shot deep-ultraviolet (DUV) KrF laser recording. As far as we are aware, this study is the first to apply HGNs in optical data storage and also the first to use a recording light source for the metal nanoparticles (NPs) that is not a surface plasmon resonance (SPR) wavelength. The short wavelength of the recording DUV laser improved the optical resolution dramatically. We prepared HGNs exhibiting two absorbance regions: an SPR peak in the near-infrared (NIR) region and an intrinsic material extinction in the DUV region. A single pulse from a KrF laser heated the HGNs and transformed them from hollow structures to smaller solid spheres. This change in morphology for the HGNs was accompanied by a significant blue shift of the SPR peak. Employing this approach, we demonstrated its patterning ability with a resolving power of a half-micrometer (using a phase mask) and developed a readout method (using a blue-ray laser microscope). Moreover, we prepared large-area, uniform patterns of monolayer HGNs on various substrates (glass slides, silicon wafers, flexible plates). If this spectral recording technique could be applied onto thin flexible tapes, the recorded data density would increase significantly relative to that of current rigid discs (*e.g.*, compact discs).

KEYWORDS: hollow gold nanoparticles · laser-induced photomodification · surface plasmon resonance · optical data storage · KrF laser

In recent years, there has been increasing interest in the unique physical and chemical properties of metal nanostructures because of their fundamental and technological applications. For example, metal nanoparticles (NPs) are attractive for their surface plasmon resonance (SPR) properties. The strong interactions of metallic NPs with incident light (*i.e.*, with the oscillating electric field) originate from the excitation of collective oscillations of conduction electrons within these particles.[1] The SPR frequencies of metal NPs can be tuned through variations in their size,[2] shape,[3] structure,[4,5] aggregate morphology,[6] and surface chemistry[7] and of the refractive index of the surrounding medium.[8]

Moreover, hollow gold NPs (HGNs) are attractive materials because of their unique structural and optical properties, including high surface areas, low densities, and tunable SPR features. In particular, HGNs exhibit a red shift of their SPR signals relative to those of solid Au colloids. The SPR wavelength depends on the ratio of the shell thickness to its diameter.[9] In addition, the SPR wavelengths of HGNs are readily tuned into the near-infrared (NIR) region, typically from 650 to 1000 nm.[10,11] This new class of metal nanostructures has a number of uses, including applications in surface-enhanced Raman scattering (SERS),[12] optical imaging,[13] and chemical sensors.[14]

Generally, physiological media (blood, water, tissue) are relatively transparent in the NIR region, allowing tissue penetration depths of up to 10 cm.[15] Because HGNs have strong SPR absorbance across the NIR window, femtosecond or nanosecond pulsed-laser irradiation can heat these HGNs sufficiently to melt and ablate the HGNs into smaller NPs, which makes them suitable for biomedical applications (*e.g.*, photothermal destruction of cancer or bacterial cells).[16−18] Much experimental and theoretical research has been performed recently to examine the pulsed-laser irradiation on HGNs.[19−24] The photophysical processes involved in this phenomenon include the laser excitation of electrons and their thermal heating due to electron−electron thermalization, the lattice heating resulting from electron−phonon relaxation, particle melting, and heat release to the surrounding medium.[20,22,23] The time scale for the heat dissipation to the embedding environment is generally on the order of hundreds of picoseconds.[25] When the width

*Address correspondence to hsuenlichen@ntu.edu.tw.

Received for review September 26, 2009 and accepted December 1, 2009.

Published online December 7, 2009. 10.1021/nn9013005

of the excitation pulse is shorter than this duration, it is possible to preferentially heat the metal lattice while maintaining the temperature of the surrounding medium. Conversely, NPs heated by continuous-wave laser irradiation transfer the absorbed energy into the surrounding medium without observable increases in NP temperature.[26,27] To our best knowledge, however, no studies of the pulsed-laser irradiation of metal NPs have been performed using wavelengths in non-SPR absorbance regions, especially the deep-ultraviolet (DUV) region ($\lambda < 300$ nm).

SPR techniques are now used routinely in a wide variety of optical data storage systems.[28−34] Aussenegg *et al.* used the shape dependence of the SPR shift of metal NPs for optical data storage through spectral coding.[28] Tsai *et al.* used the localized electric field enhancement by Ag NPs to develop near-field optical disks.[29,30] Kawata *et al.* and Gu *et al.* both combined femtosecond lasers with metal NPs as spectral coding techniques. Kawata *et al.* hybridized organic dyes and Au^{3+} ions in polymethylmethacrylate as a recording material; because the emitted fluorescence intensity of the dye could be enhanced by the Au NPs, they used femtosecond laser-irradiation-induced reduction of Au^{3+} ions to Au NPs as a writing and reading system.[31] Gu *et al.* demonstrated multicolor spectral encoding using three sizes of Au nanorods doped in a SiO_2 sol−gel matrix.[32−34] Femtosecond laser irradiation causes metal nanorods to undergo shape transformations *via* melting or fragmentation processes, resulting in significant shifts in the SPR peak; because Gu *et al.* used three sizes of Au nanorods exhibiting different SPR peaks (700, 840, and 980 nm), the data density could increase to up to 3^2 times that of the current limit.[32−34] No previous studies have been performed, however, on the application of the HGNs to optical data storage. Furthermore, the resolution of an optical imaging system is generally given by the well-known Rayleigh criterion:[35,36]

$$CD = 0.6 \times \lambda/NA$$

where CD is the critical dimension or the smallest resolvable linear dimension, λ is the optical wavelength, and NA is the numerical aperture of the optical system. Obviously, a decrease in the laser wavelength causes the resolution to decrease, resulting in a significant enhancement in data density. The central wavelengths of the common femtosecond pulsed lasers used in previous studies[32−34] have, however, been generally located in the NIR region ($\lambda = 700-1000$ nm); that is, they are longer than the recording wavelengths used in contemporary optical storage systems, such as compact discs (CDs; $\lambda = 780$ nm), digital video discs (DVDs; $\lambda = 650$ nm), and Blu-ray DVDs ($\lambda = 405$ nm). Therefore, a conventional femtosecond laser having a wavelength in the NIR region would not be the best choice for high-density optical data storage. In this study, we used a KrF laser having a wavelength located in the DUV region ($\lambda = 248$ nm) as a recording system to significantly improve the optical resolution. The International Technology Roadmap for Semiconductors (ITRS) suggested that KrF laser-based optical lithography might yield optical resolution down to 130 nm on the photoresist.[35]

Polymers are expected to play important roles in optical communications, optical data processing, photovoltaics, panel displays, and thermo-optic switching devices.[35−44] They possess several advantageous features, including the potential for cheap processing on large areas, high transparency, mechanical flexibility, and are lightweight. Polymer substrates having good luminous transmittance (*ca.* 90%) and high mechanical strength might be profitably used as rigid supporting materials for convectional CDs, DVDs, and Blu-ray DVDs. On the other hand, however, thin substrates possessing good flexibility[44] can be applied to so-called Roll-to-Roll (R2R) processing for rapid and massive-scale production.[43]

In this paper, we describe the one-shot KrF pulsed-laser-induced photomodification of self-assembled monolayer HGNs immobilized on both rigid and flexible substrates as a means for optical data storage through spectral recoding. We prepared hollow metal NPs through galvanic replacement reactions between Ag NPs and $HAuCl_4$. We employed a variety of methods, including UV−vis−NIR spectroscopy, scanning electron microscopy (SEM), and transmission electron microscopy (TEM), to investigate the changes in the optical properties and morphologies of the HGNs induced by irradiation of the KrF pulsed laser. Herein, we discuss the effects of these HGNs after one shot of pulsed-laser irradiation and the working temperature range of the data storage system. We also fabricated a periodic grating pattern through a phase mask to demonstrate the ability to pattern on the half-micrometer scale. Finally, we discuss the formation of large-area, uniform patterns on various conventional substrates (glass slides, Si wafers, flexible plates).

RESULTS AND DISCUSSION

Figure 1 illustrates the concept of spectral recording using a KrF pulsed laser. First, we prepared HGNs through the reaction of aqueous $HAuCl_4$ solutions with Ag NPs as templates.[10,14] Changing the Ag NPs-to-$HAuCl_4$ ratio allowed us to control the SPR wavelength. Then, we allowed the HGNs to self-assemble through chemical adsorption onto rigid substrates (*e.g.*, glass, quartz, Si) that we had modified to present NH_2 groups. The number density was *ca.* 150 particles μm^{-2}; the surface coverage was *ca.* 21%. To prepare HGNs on flexible substrates (*e.g.*, polycarbonate (PC) or polyethylene (PE)), we used previously published[45] reversal imprinting technology to transfer HGNs from glass slides onto

the flexible plates at temperatures below the glass transition temperatures (T_g) of the flexible materials. A single pulse of KrF laser irradiation was sufficient to heat the monolayer HGNs in the exposure region. The absorbed laser energy then led to the collapse of these HGNs into smaller solid metal NPs, with an accompanying blue shift in the SPR absorbance. It is noteworthy that we used a KrF laser in this study, rather than the femtosecond lasers that are typically used to reshape Au nanostructures.[16−24,32−34] The working wavelength can effectively be reduced from the NIR ($\lambda = 700-1000$ nm) to the DUV ($\lambda = 248$ nm) region. According to the Rayleigh criterion,[35,36] the smallest resolvable line dimension is directly proportional to the wavelength; therefore, using a KrF laser as the recording light source, rather than a femtosecond laser, could increase the data density approximately 8-fold.

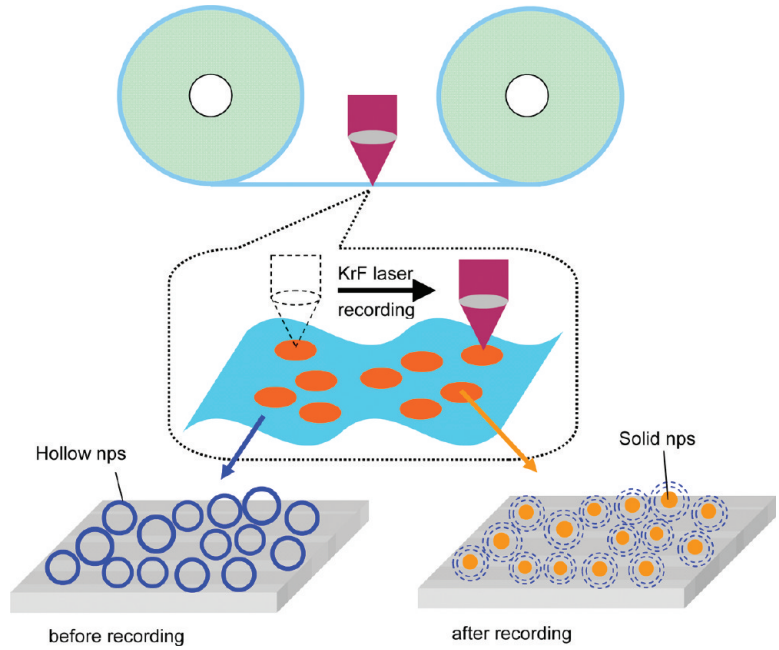

Figure 1. Schematic representation of recording mechanism through single-pulse KrF laser-induced melting of monolayer HGN-coated flexible tapes.

Figure 2a displays the TEM morphology of one HGN having a diameter of *ca.* 42 nm. The morphology could be easily controlled by changing the size of Ag NPs and the volume of $HAuCl_4$.[14] To investigate the optical behavior of the HGNs at a wavelength of 248 nm, we used a DUV-transparent quartz plate as a substrate. Figure 2b presents the transmission spectra of a quartz slide before and after deposition of the HGNs. In contrast to the blank quartz plate (solid line in Figure 2b), the quartz plate presenting the HGNs exhibited two apparent absorbance regions (dashed line in Figure 2b). We attribute the transmission dip located at *ca.* 590 nm to the SPR of the HGNs, in agreement with our results in a previous study.[14] The SPR dip was broadened because of the slight polydispersity. It is interesting that these HGNs exhibit another weaker absorbance region at wavelengths of less than 300 nm, in addition to the typical SPR absorbance. Because the blank quartz plate provided high transmission in the DUV region ($T\% > 90\%$), this absorbance must have resulted from the HGNs, possibly because of the intrinsic material extinction of the metal—for example, bulk Au and Ag both have high extinction coefficients at 248 nm (1.22 and 1.39, respectively).[46] Moreover, although little is known of the optical properties of metal NPs in the DUV region, Silva *et al.* noted the KrF nanostructuring phenomenon in thin metal films.[47] They investigated the physical mechanisms behind the KrF laser melting for a variety of metal films. It is evident that metals such as Au and Ag can effectively absorb energy from DUV lasers, resulting in melting upon KrF laser irradiation.

Figure 3a displays the absorbance spectra of the HGNs irradiated by one shot from a KrF laser at different fluences. Prior to irradiation, these samples displayed an SPR peak located at *ca.* 620 nm. This SPR peak decreased in intensity, and the absorption signals at shorter wavelengths (*ca.* 450 nm) underwent significant increases in intensity, upon increasing the fluence of the KrF laser irradiation from 9 to 22 mJ cm^{-2}. The SPR peak of the HGNs disappeared after single-pulsed irradiation at the fluence of 38 mJ cm^{-2} (yellow line in Figure 3a), indicating the almost immediate collapse of the HGNs. The SPR peak shifted to a wavelength of *ca.* 450 nm, indicating that smaller solid particles were formed after irradiation with the KrF laser. It is interesting that this blue-shifted SPR peak was not located between 500 and 550 nm, the typical range for small solid Au NPs. Note that we synthesized the HGNs through the reactions of aqueous $HAuCl_4$ solutions with Ag NPs. Generally, most HGNs are composed of reduced Au and residual Ag. For instance, the molar ratio of the HGN in Figure 2a was 60/40 (Ag/Au), as measured using energy-dispersive spectroscopy (EDS). After irradiation, the HGNs melted and transformed into smaller solid Au/Ag alloy NPs. A previous study found that the SPR peaks of Au/Ag alloy NPs of the various molar ratios were located between 420 and 520 nm.[48] Therefore, the fact that the SPR peak of our solid alloy NPs was located at *ca.* 450 nm is consistent with this range. Furthermore, the blue shift of the wavelength, compared with that of solid Au NPs, is more suitable for use as a readout wavelength because of the higher resolving power. In addition, although the initial SPR absorption band of the HGNs was broad (it was a summation of the different resonances of HGNs that were polydisperse in both shape and size), after irradiation it disappeared completely, indicating that all of the polydisperse HGNs effectively absorb the KrF laser energy in the single-pulsed duration.

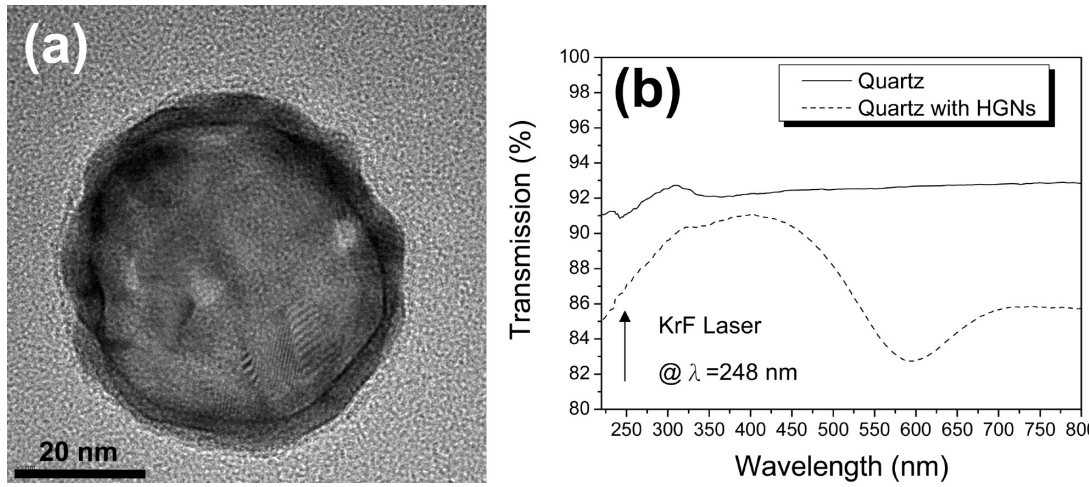

Figure 2. (a) TEM image of an HGN. (b) Transmission spectra of a quartz plate before (solid line) and after (dash line) immersion in the HGN solution.

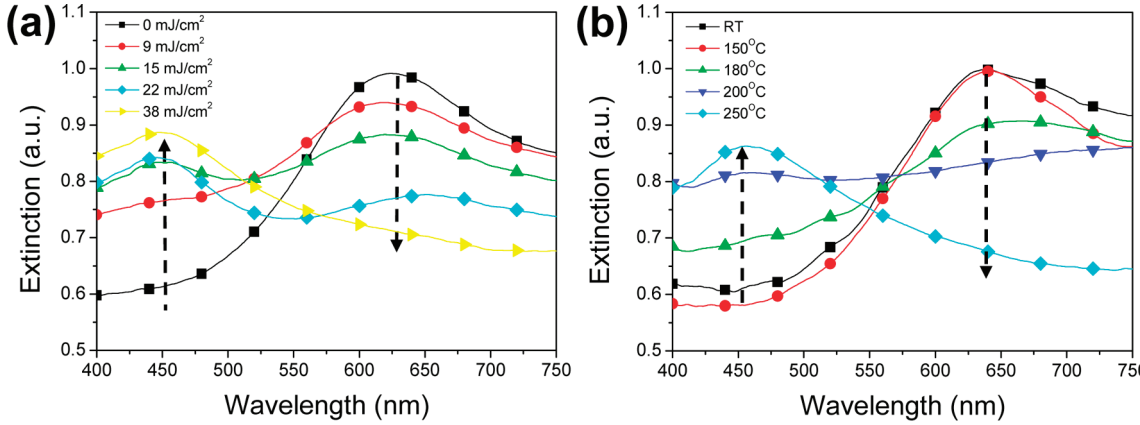

Figure 3. (a) Absorbance spectra of monolayer HGNs coated on glass slides irradiated with one shot of a KrF laser at different fluences. (b) Absorbance spectra of monolayer HGNs coated on glass slides after thermal treatment at the various temperatures for 20 min.

Our single-pulsed photomodification threshold (38 mJ cm^{-2}) was close to the values that can be extracted from the data reported for various Au nanostructures subjected to femtosecond pulses at SPR wavelengths: 10−40 mJ cm^{-2} (nanoshells with silica core),[22,23] 10 mJ cm^{-2} (nanocages),[21] 7−16 mJ cm^{-2} (nanorods),[32,33] and 10−20 mJ cm^{-2} (HGNs).[19] In our case, the threshold (38 mJ cm^{-2}) was only slightly higher than most of these values for two possible reasons: (i) the weaker absorbance at the wavelength of 248 nm is about half of the absorbance at the SPR peak for HGNs; (ii) the single pulse that we applied is much less than the number of pulses used in studies above (*e.g.*, 7.5×10^6 for nanoshells with silica cores,[22] 2.05×10^6 for nanorods,[32] and 9×10^5 for HGNs).[19] Note, however, that complete photomodification of HGNs induced by only one shot would be an outstanding advantage for increased recording speed.

To experimentally determine the actual melting temperature of these HGNs, we treated glass plates coated with HGNs at temperatures ranging from 150 to 250 °C, each for a duration of 20 min. Figure 3b displays a set of HGN extinction spectra that indicate the changes in absorbance following these heating treatments. When we increased the temperature from room temperature to 150 °C, we observed no apparent change (red line in Figure 3b). Note that the HGNs exhibited thermal stability at 150 °C, indicating that they should have maintained their original optical properties after being transferred to the flexible substrates. The SPR peaks (*ca.* 620 nm) decreased in intensity, and the absorption signals at shorter wavelengths (*ca.* 450 nm) underwent significant increases after we increased the temperature from 150 to 200 °C. The SPR peak for the HGNs disappeared after heat treatment at 250 °C (cyan line in Figure 3b), indicating that almost all of the HGNs had collapsed. This spectral phenomenon is analogous to that of the HGNs after laser irradiation (Figure 3a), also due to the melting of HGNs. Stated another way, we determined experimentally that these HGNs began to melt at 180 °C and had completely collapsed at 250 °C. This temperature is significantly below the bulk metal melting temperature of either Ag (962 °C) or Au (1064 °C). We attribute this phenomenon to the surface

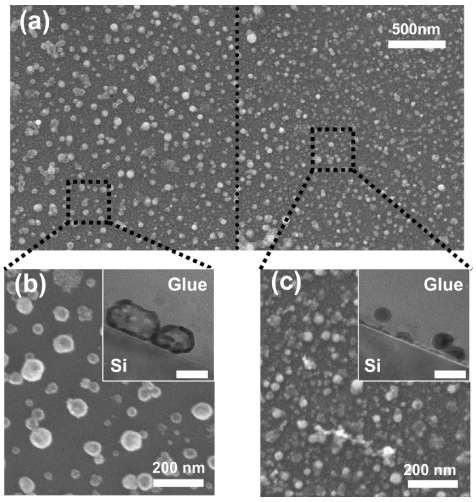

Figure 4. (a) SEM image of monolayer HGNs coated on Si wafers (left) before and (right) after irradiation with a KrF laser; (b,c) higher-magnification SEM images in (a). Inset: Cross-sectional TEM images corresponding to (b) and (c). Scale bar = 40 nm.

melting of metal nanostructures.[49,63] In such nanostructures, melting is initiated at external surfaces or along internal defects, such as grain boundaries and dislocations, and it is directly affected by changes in the surface free energy of the metal.[50,51] In our case, the HGNs had an inherently high surface-to-volume ratio because of their hollow sphere geometry; therefore, an increased percentage of surface atoms would be affected by surface-initiated melting. Also, the metallic shells were rough and contained pinholes (Figure 2a), resulting in an increased surface area and a high number of surface defects. These characteristics are all factors accentuating the melting point depression. Therefore, the real melting point of the HGNs (<250 °C) might be much lower than their actual temperature after laser irradiation, resulting in the destruction of hollow structures.

To further confirm the photomodification of the HGNs, Figure 4 displays top-view SEM and cross-section TEM images of monolayer HGNs deposited on Si wafers before and after one-shot KrF laser irradiation. In Figure 4a, the HGNs on the left of the dashed line had not been irradiated, whereas the particles on the right had. All particles were uniformly distributed over the whole surface area without obvious aggregation, consistent with our observations from the absorbance spectra in Figure 3. In the SEM images recorded at higher magnification (Figure 4b,c), it was evident that laser irradiation resulted in a reduction in the particle dimensions and an increase in the particle number density. In addition, the cross-section TEM images (insets to Figure 4b,c) revealed a distinct change in morphology from hollow spheres to smaller solid spheres after one-shot laser irradiation. It is interesting that the shapes of the HGNs were originally slightly polydisperse, but then transformed into rounder spheres having lower free energy.[49] On the basis of these results, including the absorbance spectra and morphologies of the HGNs after laser irradiation, it appears that the single-pulse KrF laser irradiation efficiently heated the HGNs and caused them to melt to form smaller solid NPs, accompanied by an obvious blue shift of the SPR peak, even though the wavelength of the KrF laser (248 nm) did not overlap with the typical SPR absorbance region for HGNs.

Next, we demonstrated that this optical data storage medium has the ability to be patterned with submicrometer resolution *via* KrF laser irradiation through a phase mask. In previous studies, KrF laser exposure through a phase mask has been demonstrated as a convenient and effective means of writing submicrometer gratings for optoelectronic device applications, including fiber Bragg gratings (FBG).[52−57] Figure 5a presents a schematic representation of KrF laser irradiation at normal incidence to the phase mask, with diffracted light split into the order of $m = 0, \pm1, \pm2$. The ideal phase mask for grating fabrication would have zero order, with all diffraction orders other than ±1 being fully suppressed, so that two beams of order ±1 interfere at the HGN monolayer having a period of the grating Λ related to the diffraction angle θ by

$$\Lambda = \frac{\lambda}{2 \sin \theta} = \frac{d}{2}$$

where d is the period of the phase mask, Λ is the period of the interference fringes, and λ is the KrF laser wavelength. Because the interference occurs at the near-field region, a phase mask can overcome the temporal coherence issue of a KrF laser. A number of re-

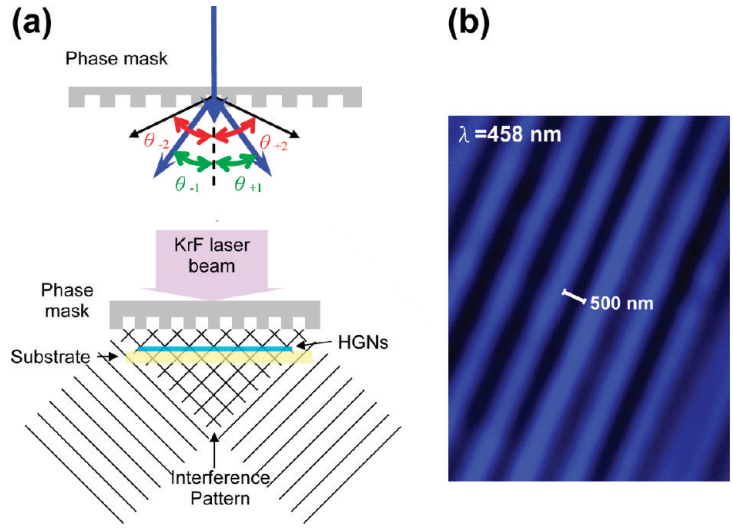

Figure 5. (a) Schematic representation of an HGN monolayer patterned *via* irradiation with KrF laser through a phase mask. (b) Transmission image (λ = 458 nm) of an HGN monolayer coated on a glass slide after irradiation with a single pulse from a KrF laser through a phase mask. The period of the phase mask was 1064 nm.

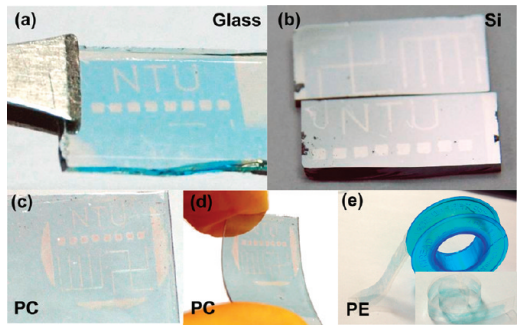

Figure 6. Photographic images of monolayer HGNs coated on a (a) glass slide, (b) Si wafer, and (c,d) PC plate; (e) PE tape recorded using irradiation from a single pulse of a KrF laser through an Al shadow mask.

ports describe how the same phase mask could produce *d*/2-spaced type I "photo-refractive" gratings and *d*-spaced type II "damage" gratings in fibers under various subsequent exposure conditions.[54−57] For low-fluence, multiple-pulse KrF laser irradiation, the gratings grow through a photosensitive effect (type I gratings); at high fluences, however, they can be produced by a single pulse, through what is believed to be a damage mechanism at the core-cladding interface (type II gratings).

Using a transmission laser microscope, we could directly verify the existence of the periodic grating pattern by observing the images of HGNs coated on glass slides irradiated by a KrF laser through a phase mask. The absorbance spectra in Figure 3a reveal that the SPR peak for the HGNs underwent a blue shift from *ca.* 620 to *ca.* 450 nm after one-shot KrF laser irradiation. They indicate that the non-irradiated HGNs were transparent, whereas the smaller solid NPs were opaque, when the incident laser light had a wavelength of 458 nm. As expected, the image (Figure 5b) appears in the form of a fringe pattern having the 1064 nm period of the phase mask and a line width of *ca.* 500 nm; the bright blue region represents the original HGNs, and the dark region indicates the photoinduced smaller solid NPs formed through the single pulse of the KrF laser. The high contrast in the fringe pattern reveals that a large photoinduced spectral change occurred to the HGNs. There are two possible reasons why we did not observe a grating having a period of *d*/2: (i) our system was a type of damage grating (type II) because the KrF laser irradiation directly resulted in the complete collapse of all of the HGNs; (ii) spatial resolution limitations of the optical microscope made it difficult to observe the existence of a grating having the period of *d*/2. Most importantly, we could quickly read out the recorded data (the signal of the solid NPs) on the half-micrometer scale by using a transmission laser microscope.[32−34]

Figure 6 presents photographic images of large-area patterned HGNs self-assembled on glass slides, Si wafers, and flexible plates. All of these substrates presenting HGNs were cut into *ca.* 1.5 cm × 1.5 cm pieces and irradiated directly with a single pulse from a KrF laser through an Al shadow mask. Clear letters and symbols were patterned uniformly on all samples. Interestingly, the threshold fluences for the various substrates were surprisingly close, presumably because these HGNs were located on the surfaces and absorbed the laser energy prior to the heat arriving on the substrates. Moreover, although the substrates also absorbed the residual light and heat, we observed no distinct destruction, indicating no obvious temperature increase. In addition, because the submicrometer scale patterning technology could be applied to HGNs on various kinds of substrates (Figure 6), it has the potential to be combined with a series of SPR applications, such as bio/chemical sensors, surface-enhanced Raman spectroscopy, metal-enhanced fluorescence, and photovoltaic cells.[58−61]

Figure 6d,e displays the HGN-coated surfaces of flexible PC and PE substrates, respectively, indicating that we could fabricate flexible optical data storage systems with dramatically enhanced data intensity relative to those of current rigid discs. For example, we could use the R2R process to fabricate an "NP tape" having the same appearance and volume as a conventional DVD by using a thin flexible belt having a thickness of 4 μm[42] and a width of 1200 μm (the typical thickness of a DVD). This system would greatly raise the active recording area by up to 300 times that of a DVD because the DVD only records data on one middle layer. Furthermore, recording onto the HGN-doped NP tape through a KrF laser (248 nm) would increase the data density to *ca.* 3000 times that of a CD (780 nm) or *ca.* 800 times that of a Blu-ray DVD (405 nm). Besides, our method is especially worthy and suitable for long-term, large-data storage requirement because our HGNs might have a better stability under atmosphere than organic dyes used in a CD or DVD.[64] Future studies will be aimed at improving both the recording and readout systems. First, it might be possible to replace the KrF laser (248 nm) with an ArF laser (193 nm) to improve the recording solving power. Moreover, the resolution might move down to single-nanoparticle scale (<100 nm) if our method could be improved by using the so-called "resolution enhancement techniques (RETs)" generally used in semiconductor industry.[65,66] Second, because the readout resolution was limited to *ca.* 450 nm by the SPR wavelength of the solid Ag/Au alloy NPs, it might be improved by replacing the hollow Au spheres with hollow Pt spheres[5] because solid Pt NPs having diameters of 10−30 nm feature an SPR signal in the DUV region.[62]

CONCLUSIONS

We performed a detailed investigation into the one-shot KrF pulsed-laser-induced photomodification of self-assembled monolayer HGNs immobilized on rigid and flexible substrates and then used the photomodifi-

cation phenomenon of HGNs to demonstrate its potential applicability to optical data storage through spectral recoding. We prepared the HGNs through galvanic replacement reactions between Ag NPs and $HAuCl_4$. These HGNs absorb in two distinct regions: a typical SPR peak in the vis−NIR region and a metal intrinsic absorption in the DUV region. The HGNs absorbed the energy from a single pulse of KrF laser irradiation with a threshold fluence of 38 mJ cm^{-2}, causing the effective heating and collapse of the HGNs. The absorbed energy resulted in the temperature rising to above the experimentally determined melting point of the HGNs; it then transformed the geometry of the HGNs from hollow spheres to smaller solid spheres. The collapse of the HGNs was accompanied by an obvious blue shift of the SPR peak from 620 to 450 nm. Therefore, the KrF laser-induced absorbance change could be used as a readout when using a blue-ray transmission laser microscope. We also recorded a periodic grating pattern onto the HGNs through a phase mask to demonstrate the half-micrometer storage ability. Finally, we recorded HGN patterns uniformly on various large-area substrates, namely, glass slides, Si wafers, and flexible plates. We suspect that, if the proposed method were to be applied to recording on an HGN-coated tape, the data density would increase greatly—possibly to over 10^3 times that available on convectional rigid discs.

METHODS

Materials. All chemicals were used as received, without any further purification. Sodium citrate (99%), silver nitrate ($AgNO_3$, 99%), hydrogen tetrachloroaurate ($HAuCl_4$, 99.999%), polyvinylpyrrolidone (PVP, M_w = *ca.* 30k), 3-aminopropyltrimethoxysilane (APTMS), methanol (MeOH, 99.5%), ethanol (EtOH, 99.8%), and ethylene glycol (EG, 99.8%) were obtained from ACROS. Si wafers and quartz plates were obtained from SummitTech Co. PC plates having a thickness of 380 μm and PE tapes having a thickness of 40 μm were obtained from PERM TOP Co., Ltd.

Colloid Preparation. HGNs were prepared through the reaction of $HAuCl_4$ with Ag NPs, according to a method published previously.[14] Briefly, $AgNO_3$ (0.04 g) and PVP (1 g) were dissolved in EG (20 mL). This mixture was heated at 160 °C for 2 h under vigorous magnetic stirring and then cooled to room temperature. The resulting Ag colloid prepared using the polyol method formed stable dispersions in water without the need to add additional stabilizers. The solution of the Ag NPs (1 mL) was diluted in deionized water (25 mL) and then heated under reflux for 10 min before 2 mM the aqueous $HAuCl_4$ (1.5 mL) was added dropwise. After 20 min of stirring, the particles were cooled to room temperature, purified through gradient centrifugation, washed twice with 0.3 mM aqueous sodium citrate, redispersed in 0.3 mM sodium citrate (5 mL), and finally stored at 4 °C.

HGN Monolayer Preparation. Clean, polished solid substrates (quartz, glass, Si) were immersed for 45 min in a boiling solution of 2% (v/v) of APTMS in anhydrous EtOH. The substrates were then rinsed thoroughly with MeOH to remove any unbound monomer from the surface. At this point, the silanized substrates were stored in MeOH until required. Prior to derivatization with colloidal NPs, the substrates were rinsed with ultrapure water (UPW) and immersed in vials of NPs for 2 h (glass, quartz) or 6 h (Si). The NP-deposited substrates were then spun at 3000 rpm to remove any excess NPs. After performing a final UPW rinse, the samples were dried and stored under ambient conditions until required for further use. Using reversal imprinting technology[45] and an imprinter, the monolayer HGNs were transferred from the glass slides onto flexible plates under a pressure of 6 MPa at a temperature of 150 °C (PC) or 100 °C (PE) for 5 min. After cooling to room temperature, the samples were stored under ambient conditions until required for further use.

Laser Irradiation and Heat Treatment. For recording, the sample was irradiated with a KrF excimer pulsed laser (Lamda Physik, Compex 150T, 248 nm) emitting a 20 ns pulse. Typically, our single-pulsed threshold fluence to melt the HGNs completely ranged from 35 to 40 mJ cm^{-2}. The slight fluctuation in threshold was attributed to the HGNs being polydisperse in both shape and size for our samples. Submicrometer patterning was performed using a fused silica phase mask (StockerYale) featuring a one-dimensional surface relief pattern (square grating, 10 × 20 mm, 1.06 μm period). The phase mask was directly in contact with HGN-modified samples, and the single-pulsed (20 ns) threshold fluence of 40 mJ cm^{-2} was used. For heat treatment, the samples were placed in an oven for 20 min, preheated at various temperatures from 150 to 250 °C, and then they were cooled to room temperature.

Characterization. Readout of the recorded periodic grating was performed using a transmission laser microscope (Leica TCS-SP2, 458 nm); samples were observed through a 100×, 1.40 NA oil immersion objective. The absorption spectra were measured using a Hitachi U4100 optical spectrometer. Cross-sectional views and EDS analyses of the NPs were performed using a Philips Tecnai F20 G^2 field emission transmission electron microscope (FEI-TEM). The NP-deposited substrates were observed using a JEOL JSM-6500F scanning electron microscope.

Acknowledgment. We thank the National Science Council, Taiwan, for supporting this study under Contracts NSC-97-2221-E-002-046-MY3 and NSC-97-2623-7-002-008-ET.

REFERENCES AND NOTES

1. Kelly, K. L.; Coronado, E.; Zhao, L. L.; Schatz, G. C. The Optical Properties of Metal Nanoparticles: The Influence of Size, Shape, and Dielectric Environment. *J. Phys. Chem. B* **2003**, *107*, 668–677.
2. Yguerabide, J.; Yguerabide, E. E. Light-Scattering Submicroscopic Particles as Highly Fluorescent Analogs and Their Use as Tracer Labels in Clinical and Biological Applications. *Anal. Biochem.* **1998**, *262*, 137–156.
3. Orendorff, C. J.; Sau, T. K.; Murphy, C. J. Shape-Dependent Plasmon-Resonant Gold Nanoparticles. *Small* **2006**, *2*, 636–639.
4. Jackson, J. B.; Halas, N. J. Silver Nanoshells: Variations in Morphologies and Optical Properties. *J. Phys. Chem. B* **2001**, *105*, 2743–2746.
5. Selvakannan, P. R.; Sastry, M. Hollow Gold and Platinum Nanoparticles by a Transmetallation Reaction in an Organic Solution. *Chem. Commun.* **2005**, 1684–1686.
6. Novak, J. P.; Nickerson, C.; Franzen, S.; Feldheim, D. L. Purification of Molecularly Bridged Metal Nanoparticle Arrays by Centrifugation and Size Exclusion Chromatography. *Anal. Chem.* **2001**, *73*, 5758–5761.
7. Caruso, R. A.; Antonietti, M. Sol−Gel Nanocoating: An Approach to the Preparation of Structured Materials. *Chem. Mater.* **2001**, *13*, 3272–3282.
8. Kubo, S.; Diaz, A.; Tang, Y.; Mayer, T. S.; Khoo, I. C.; Mallouk, T. E. Tunability of the Refractive Index of Gold Nanoparticle Dispersions. *Nano Lett.* **2007**, *7*, 3418–3423.
9. Hao, E.; Li, S.; Bailey, R. C.; Zou, S.; Schatz, G. C.; Hupp, J. T. Optical Properties Of Metal Nanoshells. *J. Phys. Chem. B* **2004**, *108*, 1224–1229.
10. Sun, Y. G.; Xia, Y. N. Increased Sensitivity of Surface Plasmon Resonance of Gold Nanoshells Compared to That

of Gold Solid Colloids in Response to Environmental Changes. *Anal. Chem.* **2002**, *74*, 5297–5305.
11. Sun, Y G.; Xia, Y. N. Mechanistic Study on the Replacement Reaction between Silver Nanostructures and Chloroauric Acid in Aqueous Medium. *J. Am. Chem. Soc.* **2004**, *126*, 3892–3901.
12. Schwartzberg, A. M.; Oshiro, T. Y.; Zhang, J. Z.; Huser, T.; Tally, C. E. Improving Nanoprobes Using Surface-Enhanced Raman Scattering from 30-nm Hollow Gold Particles. *Anal. Chem.* **2006**, *78*, 4732–4736.
13. Shukla, S.; Priscilla, A.; Banerjee, M.; Bhonde, R. R.; Ghatak, J.; Satyam, P. V.; Sastry, M. Porous Gold Nanospheres by Controlled Transmetalation Reaction: A Novel Material for Application in Cell Imaging. *Chem. Mater.* **2005**, *17*, 5000–5005.
14. Wan, D. H.; Chen, H. L.; Lin, Y. S.; Chuang, S. Y.; Shieh, J.; Chen, S. H. Using Spectroscopic Ellipsometry To Characterize and Apply the Optical Constants of Hollow Gold Nanoparticles. *ACS Nano* **2009**, *3*, 960–970.
15. Weissleder, R. A Clearer Vision for *In Vivo* Imaging. *Nat. Biotechnol.* **2001**, *19*, 316–317.
16. Chen, J.; Saeki, F.; Wiley, B. J.; Cang, H.; Cobb, M. J.; Li, Z. Y.; Au, L.; Zhang, H.; Kimmey, M. B.; Li, X.; Xia, Y. Gold Nanocages: Bioconjugation and Their Potential Use as Optical Imaging Contrast Agents. *Nano Lett.* **2005**, *5*, 473–477.
17. Hirsch, L. R.; Stafford, R. J.; Bankson, J. A.; Sershen, S. R.; Rivera, B.; Price, R. E.; Hazle, J. D.; Halas, N. J.; West, J. L. Nanoshell-Mediated Near-Infrared Thermal Therapy of Tumors under Magnetic Resonance Guidance. *Proc. Natl. Acad. Sci. U.S.A.* **2003**, *100*, 13549–13554.
18. Chen, J. Y.; Wiley, B.; Li, Z. Y.; Campbell, D.; Saeki, F.; Cang, H.; Au, L.; Lee, J.; Li, X. D.; Xia, Y. Gold Nanocages: Engineering Their Structure for Biomedical Applications. *Adv. Mater.* **2005**, *17*, 2255–2261.
19. Prevo, B. G.; Esakoff, S. A.; Mikhailovsky, A.; Zasadzinski, J. A. Scalable Routes to Gold Nanoshells with Tunable Sizes and Response to Near-Infrared Pulsed-Laser Irradiation. *Small* **2008**, *4*, 1183–1195.
20. Akchurin, G. B.; Khlebtsov; Akchurin, G.; Tuchin, V.; Zharov, V.; Khlebtsov, N. Gold Nanoshell Photomodification under a Single-Nanosecond Laser Pulse Accompanied by Color-Shifting and Bubble Formation Phenomena. *Nanotechnology* **2008**, *19*, 015701–015708.
21. Hu, M.; Petrova, H.; Chen, J.; McLellan, J. M.; Siekkinen, A. R.; Marquez, M.; Li, X.; Xia, Y.; Hartland, G. V. Ultrafast Laser Studies of the Photothermal Properties of Gold Nanocages. *J. Phys. Chem. B* **2006**, *110*, 1520–1524.
22. Aguirre, C. M.; Moran, C. E.; Young, J. F.; Halas, N. J. Laser-Induced Reshaping of Metallodielectric Nanoshells under Femtosecond and Nanosecond Plasmon Resonant Illumination. *J. Phys. Chem. B* **2004**, *108*, 7040–7045.
23. Prasad, V.; Mikhailovsky, A.; Zasadzinski, J. A. Inside-Out Disruption of Silica/Gold Core−Shell Nanoparticles by Pulsed Laser Irradiation. *Langmuir* **2005**, *21*, 7528–7532.
24. Harris, N.; Ford, M. J.; Cortie, M. B. Optimization of Plasmonic Heating by Gold Nanospheres and Nanoshells. *J. Phys. Chem. B* **2006**, *110*, 10701–10707.
25. Link, S.; Hathcock, D. J.; Nikoobakht, B.; El-Sayed, M. A. Medium Effect on the Electron Cooling Dynamics in Gold Nanorods and Truncated Tetrahedra. *Adv. Mater.* **2003**, *15*, 393–396.
26. Roper, D. K.; Ahn, W.; Hoepfer, M. Microscale Heat Transfer Transduced by Surface Plasmon Resonant Gold Nanoparticles. *J. Phys. Chem. C* **2007**, *111*, 3636–3641.
27. Richardson, H. H.; Hickman, Z. N.; Govorov, A. O.; Thomas, A. C.; Zhang, W.; Kordesch, M. E. Thermooptical Properties of Gold Nanoparticles Embedded in Ice: Characterization of Heat Generation and Melting. *Nano Lett.* **2006**, *6*, 783–788.
28. Ditlbacher, H.; Krenn, J. R.; Lamprecht, B.; Leitner, A.; Aussenegg, F. R. Spectrally Coded Optical Data Storage by Metal Nanoparticles. *Opt. Lett.* **2000**, *25*, 563–565.
29. Shi, L. P.; Chong, T. C.; Yao, H. B.; Tan, P. K.; Miao, X. S. Super-Resolution Near-Field Optical Disk with an Additional Localized Surface Plasmon Coupling Layer. *J. Appl. Phys.* **2002**, *91*, 10209–10211.
30. Ng, M. Y.; Liu, W. C. Super-Resolution and Frequency-Dependent Efficiency of Near-Field Optical Disks with Silver Nanoparticles. *Opt. Express* **2005**, *13*, 9422–9430.
31. Tanaka, T.; Kawata, S. Three-Dimensional Multilayered Optical Memory Using Two-Photon Induced Reduction of Au^{3+} Doped on PMMA. *IEEE Trans. Magn.* **2007**, *43*, 828–831.
32. Zijlstra, P.; Chon, J. W. M.; Gu, M. Effect of Heat Accumulation on the Dynamic Range of a Gold Nanorod Doped Polymer Nanocomposite for Optical Laser Writing and Patterning. *Opt. Express* **2007**, *15*, 12151–12160.
33. Chon, J. W. M.; Bullen, C.; Zijlstra, P.; Gu, M. Spectral Encoding on Gold Nanorods Doped in a Silica Sol−Gel Matrix and Its Application to High-Density Optical Data Storage. *Adv. Funct. Mater.* **2007**, *17*, 875–880.
34. Zijlstra, P.; Chon, J. W. M.; Gu, M. Five-Dimensional Optical Recording Mediated by Surface Plasmons in Gold Nanorods. *Nature* **2009**, *459*, 410–413.
35. Smith, S. F. G.; Thomson, J. H. *Optics*; Wiley: New York, 1988; pp 214−215.
36. Kuznetsova, Y.; Neumannm, A.; Brueck, S. R. J. Imaging Interferometric Microscopy-Approaching the Linear Systems Limits of Optical Resolution. *Opt. Express* **2007**, *15*, 6651–6663.
37. Mohlmann, G. R. Developments of Optically Nonlinear Polymers and Devices. *Synth. Met.* **1990**, *37*, 207–221.
38. Stegeman, G. I.; Seaton, C. T. Nonlinear Integrated Optics. *J. Appl. Phys.* **1985**, *58*, 57–78.
39. Tripathi, K. N.; Sharma, V. K.; Kapoor, A. Polymeric Optical Waveguide Polarizer/Mode Filter with Low Index Dielectric Buffer Layer. *Int. Electromag. Compatibility Symp.* **1992**, *173*, 92–95.
40. Singer, K. D.; Kuzyk, M. G.; Holland, W. R.; Sohn, J. E.; Lalma, S. J.; Conizzoli, R. B.; Hatz, H. E.; Schilling, M. L. Electro-Optic Phase Modulation and Optical Second-Harmonic Generation in Corona-Poled Polymer Films. *Appl. Phys. Lett.* **1988**, *53*, 1800–1802.
41. Kapoor, S. K.; Pandey, C. D.; Joshi, J. C.; Dawar, A. L.; Tripathi, K. N.; Gupta, V. L. Polyurethane Coating for Integrated Optic Applications. *Thin Solid Films* **1988**, *161*, 79–81.
42. Ghawana, K.; Singh, S.; Sharma, V. K.; Kapoor, A.; Tripathi, K. N. Dip-Coated Thin-Film Polycarbonate Optical Waveguides. *Appl. Opt.* **1998**, *37*, 4051–4053.
43. Lungenschmieda, C.; Dennlera, G.; Neugebauera, H.; Sariciftcia, S. N.; Glatthaarb, M.; Meyerc, T.; Meyerc, A. Flexible, Long-Lived, Large-Area, Organic Solar Cells. *Sol. Energy Mater. Sol. Cells* **2007**, *91*, 379–384.
44. Zhou, L.; Wanga, A.; Wu, S. C.; Sun, J.; Park, S.; Jackson, T. N. All-Organic Active Matrix Flexible Display. *Appl. Phys. Lett.* **2006**, *88*, 083502−083504.
45. Chen, H. L.; Chuang, S. Y.; Lee, W. H.; Kuo, S. S.; Su, W. F.; Ku, S. L.; Chou, Y. F. Extraordinary Transmittance in Three-Dimensional Crater, Pyramid, and Hole-Array Structures Prepared through Reversal Imprinting of Metal Films. *Opt. Express* **2009**, *17*, 1636–1645.
46. Palik, E. D.; Ghosh, G. *Handbook of Optical Constants of Solids*; Academic: Orlando, 1985; Vol. 1; pp 286−294 and 350−356.
47. Henley, S. J.; Carey, J. D.; Silva, S. R. P. Metal Nanoparticle Production by Pulsed Laser Nanostructuring of Thin Metal Films. *Appl. Surf. Sci.* **2007**, *253*, 8080–8085.
48. Link, S.; Wang, Z. L.; El-Sayed, M. A. Alloy Formation of Gold−Silver Nanoparticles and the Dependence of the Plasmon Absorption on Their Composition. *J. Phys. Chem. B* **1999**, *103*, 3529–3533.
49. Radloff, C.; Halas, N. J. Enhanced Thermal Stability of Silica-Encapsulated Metal Nanoshells. *Appl. Phys. Lett.* **2001**, *79*, 674–676.
50. Castro, T.; Reifenberger, R.; Choi, E.; Andres, R. P. Size-Dependent Melting Temperature of Individual

Nanometer-Sized Metallic Clusters. *Phys. Rev. B* **1990**, *42*, 8548–8556.
51. Buffat, P.; Borel, J. Size Effect on The Melting Temperature of Gold Particles. *Phys. Rev. A* **1976**, *13*, 2287–2298.
52. Hosono, H.; Kurita, M.; Kawazoe, H. Excimer Laser Crystallization of Amorphous Indium-Tin Oxide Thin Flms and Application to Fabrication of Bragg Gratings. *Thin Solid Films* **1999**, *351*, 137–140.
53. B, A.; Tahir, J.; Ali, R. A. Rahman Fabrication of Fiber Grating by Phase Mask and Its Sensing Application. *J. Optoelectron. Adv. Mater.* **2006**, *8*, 1604–1609.
54. Dyer, P. E.; Farley, R. J.; Giedl, R. Analysis of Grating Formation with Excimer Laser Irradiated Phase Masks. *Opt. Commun.* **1995**, *5*, 327–334.
55. Archambault, J. L.; Reekie, L.; Russell, P. St. J. 100% Reflectivity Bragg Reflectors Produced in Optical Fibers by Single Excimer Laser Pulses. *Electron. Lett.* **1993**, *29*, 453–455.
56. Malo, B.; Johnson, D. C.; Bilodeau, F.; Albert, J.; Hill, K. O. Single-Excimer-Pulse Writing of Fiber Gratings by Use of a Zero-Order Nulled Phase Mask: Grating Spectral Response and Visualization of Index Perturbations. *Opt. Lett.* **1993**, *18*, 1277–1279.
57. Smelser, W.; Mihailov, S. J.; Grobnic, D. Formation of Type I-IR and Type II-IR Gratings with an Ultrafast IR Laser and a Phase Mask. *Opt. Express* **2005**, *13*, 5377–5386.
58. Shankar, S. S.; Rizzello, L.; Cingolani, R.; Rinaldi, R.; Pompa, P. P. Micro/Nanoscale Patterning of Nanostructured Metal Substrates for Plasmonic Applications. *ACS Nano* **2009**, *3*, 893–900.
59. Sundararajan, S. P.; Grady, N. K.; Mirin, N.; Halas, N. J. Nanoparticle-Induced Enhancement and Suppression of Photocurrent in a Silicon Photodiode. *Nano Lett.* **2008**, *8*, 624–630.
60. Ko, H.; Singamaneni, S.; Tsukruk, V. V. Nanostructured Surfaces and Assemblies as SERS Media. *Small* **2008**, *4*, 1576–1599.
61. Chaua, L. K.; Lin, Y. F.; Chenga, S. F.; Lin, T. J. Fiber-Optic Chemical and Biochemical Probes Based on Localized Surface Plasmon Resonance. *Sens. Actuators, B* **2006**, *113*, 100–105.
62. Bigall, N. C.; Hartling, T.; Klose, M.; Simon, P.; Eng, L. M.; Eychmoller, A. Monodisperse Platinum Nanospheres with Adjustable Diameters from 10 to 100 nm: Synthesis and Distinct Optical Properties. *Nano Lett.* **2008**, *8*, 4588–4592.
63. Inasawa, S.; Sugiyama, M.; Yamaguchi, Y. Laser-Induced Shape Transformation of Gold Nanoparticles below the Melting Point: The Effect of Surface Melting. *J. Phys. Chem. B* **2005**, *109*, 3104–3111.
64. Slattery, O.; Lu, R.; Zheng, J.; Byers, F.; Tang, X. Stability Comparison of Recordable Optical Discs—A Study of Error Rates in Harsh Conditions. *J. Res. Natl. Inst. Stand. Technol.* **2004**, *109*, 517–524.
65. Lai, F. D. High-Transmittance Attenuated Phase-Shift Masks Using Three-Stack $(Ta_2O_5)_x/(Al_2O_3)_{1-x}$ Coatings for the 90 nm-Technology Node. *Microelectron. Eng.* **2004**, *73−74*, 63–68.
66. Lin, C. M.; Loong, W. A. The Simulation of Application of High Transmittance AttPSM for Sub-100 nm Pattern in 248 nm Lithography. *Microelectron. Eng.* **2001**, *57−58*, 41–48.